燃烧科学与技术
Journal of Combustion Science and Technology
2024,30(5):507-519
DOI 10.11715/rskxjs.R202408008

生物质棒稳态阴燃数值分析

赵文涛，于光鑫，张　毅，王有镪，周　丹，何　芳
（山东理工大学交通与车辆工程学院，淄博 255049）

摘　要：明确生物质稳态阴燃机理是其技术应用的关键. 本文对自制生物质棒的稳态阴燃过程进行了数值分析. 在根据经验关联式计算的传播速度基础上，建立了一个同时考虑炭氧化及热解的二维稳态阴燃模型. 利用生物质棒阴燃实验对该模型进行了验证，传播速度及炭锥高度实验值与预测值的最大误差均小于 31%. 参数敏感性分析发现，随着棒状燃料直径的增加，传播速度显著降低，氧化及热解区显著增加.

关键词：稳态阴燃；生物质棒；数值分析；二维稳态模型；敏感性分析
中图分类号：TK6　　**文献标志码**：A　　**文章编号**：1006-8740(2024)05-0507-13

Numerical Analysis of Steady Smoldering of Biomass Rods

Zhao Wentao，Yu Guangxin，Zhang Yi，Wang Youtang，Zhou Dan，He Fang
(School of Transportation and Vehicle Engineering, Shandong University of Technology, Zibo 255049, China)

Abstract：Understanding the steady mechanism of biomass smoldering plays a great role in the utilization of smoldering technology. In this study numerical analysis of steady smoldering of biomass rods was performed. A two-dimensional (2D) steady model taking into account both char oxidation and pyrolysis was developed on the basis of a calculated propagation velocity according to empirical correlation. The model was validated against the smoldering experiment of biomass rods under natural conditions, and the maximum error was smaller than 31%. Parameter sensitivity analysis found that propagation velocity decreases significantly while oxidation area and pyrolysis zone increase significantly with the increasing diameter of rod fuel.

Keywords：steady smoldering; biomass rod; numerical analysis; 2D steady model; sensitivity analysis

Smoldering is a slow, low-temperature, and complex combustion phenomenon[1-3], sustained by the heat evolved when oxygen directly attacks the surface of a condensed-phase fuel[4]. Smoldering is emerging as a viable waste-to-energy approach[5] and has been used in the investigations of the energy-efficient utilization technique for organic solid wastes, such as bio-solid sewage sludge[6-7], bio-waste[8-9], oil sludge[10], food waste[11], etc.

Transient smoldering[12-16] and steady smoldering[17-18] are normally two typical cases. Most smoldering in fire[19-20], batch experiments[21-22], and heating facilities[23] is transient. Conversely, the smoldering of mosquito coils[24] and incense[25] is very close to steady

收稿日期：2024-02-07.
基金项目：中德合作交流互访资助项目(M-0183)；山东省自然科学基金资助项目(ZR2022ME038)；科技型中小企业创新能力提升工程资助项目(2021TSGC1114).
作者简介：赵文涛(1998—　　)，男，硕士研究生，zwtaow@163.com.
通信作者：何　芳，女，博士，教授，hf@sdut.edu.cn.

smoldering, which can be used for insect repellent[26], sterilization[27], and treatment of disease[28-29], etc. In addition, as to larger-scale application, steady smoldering is more suitable for smoke treatment and meets the heating needs of different heat loads. Therefore, seeking the ways to realize steady smoldering is of extreme importance for the application of smoldering.

Steady smoldering has been investigated both experimentally and theoretically, mostly focused on rod materials[30-31]. The influence of some parameters on smoldering, such as airflow rate, ash content, oxygen content, and oxygen partial pressure was emphasized in most experimental investigations. Mukunda et al[32] investigated the effects of different air flow rates (0—7 m/s) and oxygen content (23% — 44%) on incense smoldering. It was found that the propagation velocity increases with the increase of airflow rate and oxygen content in the concurrent smoldering, and there is a peak value in the opposed smoldering. Yan et al[33] recorded the char cone shape in smoldering of char rods with different ash content, and found that the char cone height is proportional to the mass flow rate of carbon. Lin et al[18] found that smoldering is oxygen controlled, thermal controlled, and chemical controlled with increasing air flow rate. Yamazaki et al[34] found that the flame does not occur in smoldering of incense when the oxygen partial pressure is lower than 0.3.

Over the past few decades, some sophisticated theoretical studies help the mechanism understanding of steady smoldering. For example, Yamazaki et al[30] applied a simplified oxidative model to reproduce the temperature in oxidation region of incense stick. It was found that the temperature gradient decreased with decreasing pressure. Kadowaki et al[35] established a 1D model for steady smoldering of rod fuel and explained the extinction due to the limitation of char oxidation rate. Rostami et al[36] developed a 2D transient model based on the first principles of natural smoldering of cigarette. The computation described the transient process from ignition to steady stage.

Nowadays, there are few theoretical studies on steady smoldering, and those previous theoretical studies mainly focused on the 1D steady or 2D transient model of steady smoldering of biomass rods, which have made indelible contributions to understanding the mechanism of steady smoldering. However, 1D steady model dose not reproduce multiple physical fields, and 2D transient model is very complex and will cost a lot of computer resources. Due to the fact that the steady stage occupies most time of the whole smoldering process for rod fuel, the key to better understanding the mechanism of steady smoldering is to find a novel way to simplify the theoretical description and reproduce the multiple physical fields in the steady stage of steady smoldering.

The objective of this study is to numerically analyze the steady smoldering of biomass rods. A steady 2D model was developed based on the calculated propagation velocity, and validated against the experiments. Then sensitivity analyses were performed to understand the effects of parameters on smoldering characteristics.

1 Model and numerical method

1.1 Simplified physical model and assumptions

1.1.1 Smoldering process

Schematic diagram and control volume of the 2D model for steady smoldering are shown in Fig.1. There are five zones from top to bottom in solid computational domain: ash rod, char oxidation surface, char cone, pyrolysis zone, and original fuel.

The smoldering propagates downwards at a constant velocity. Residual ash rod above the char oxidation surface works as insulation, and it will collapse after accumulating to a certain length. Oxidation reaction occurs on the surface of char cone (char oxidation surface) and heat generated is partially used for the pyrolysis of original fuel below, forming the pyrolysis zone. The fume produced by char oxidation and pyrolysis escapes to the surrounding of the biomass rod to form the fume layer, and the fume flows upwards.

1.1.2 Physical model

Reaction: In solid, there are two main reactions: char oxidation and pyrolysis. The char oxidation occurs on the surface of char cone, generating CO and CO_2. The pyrolysis occurs below the char cone, and the fuel is pyrolyzed into gases and char.

Mass transfer: The fume generated by the char oxidation and pyrolysis volatiles leave the reaction area via pressure driven flow and diffusion. Oxygen goes to the oxidation area (surface area of char cone) from the

surrounding via diffusion. The solid phase enters the control volume at smoldering propagation velocity u_{sm}.

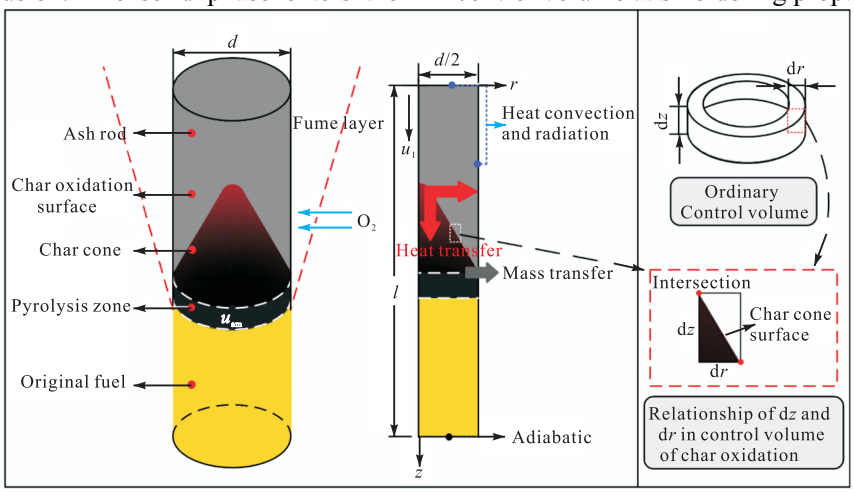

Fig.1 Schematic diagram and control volumes of the 2D steady smoldering

Heat transfer: The smoldering of the whole biomass rod is sustained by the heat released from char oxidation. The heat generated is transferred in the radial and axial directions through heat conduction. There is heat sink in pyrolysis zone. It should be noted that part of heat is entrained out due to the outflow of generated fume. Heat is transferred via convection and radiation at the top and on the cylindrical surface.

1.1.3 Coordinate system and control volume

A moving cylindrical coordinate system attached to the moving reaction front is chosen for analysis. Its moving velocity (u_1) was equal to the smoldering propagation velocity. According to different reactions and the mass / heat transfer characteristic, the interior of physical model is divided into four kinds of cylindrical ring control volumes: char oxidation, pyrolysis, ash outside char cone, and other control volumes.

The cylindrical ring control volume of physical model is shown in Fig.1. In the control volume of char oxidation, there is a special relationship of dz and dr to make sure that the boundary of the control volumes is the intersection of the char cone and cylindrical ring control volume.

1.1.4 Assumptions

The simplified mathematical description of the process in the following section is based on the following assumptions: ①No shrinkage of rods. ②Local heat equilibrium. ③Steady smoldering along the z-axis. ④Fume goes out from solid along the r-axis. ⑤Char oxidation occurs on the surface. ⑥Char cone is composed of ash and carbon. ⑦The convective heat transfer coefficient and emissivity of the top and cylindrical surface are constant. ⑧The bottom surface is adiabatic.

1.2 Mathematical model

1.2.1 Governing equations

Mass conservation: The mass of solid and gas phase in the moving control volume is kept constant in a steady state. Consequently, the rate of change is equal to the net inlet flux as shown in Eqs. (1) and (2).

$$\text{Solid}: \frac{\partial \rho_s}{\partial z} u_{sm} = \dot{\omega}_s \tag{1}$$

$$\text{Gas}: \frac{\partial (\rho_{fume} u_{fume})}{\partial r} = \dot{\omega}_{fume} \tag{2}$$

where ρ_s and ρ_{fume} are the density of solid and fume (kg/m^3), respectively; $\dot{\omega}_s$ and $\dot{\omega}_{fume}$ are the mass source of solid and fume (kg/(m^3 · s)), respectively; u_{fume} is the velocity of fume (m/s).

Energy conservation: The heat energy in the control volume is also kept constant in a steady state. It means that the sum of convection heat flux of solid in the z direction, the convection heat flux of fume in the r direction, the effective heat conduction flux in the z and r directions, and the heat source rate is zero.

$$\frac{\partial (\rho_s u_{sm} c_s T)}{\partial z} + \frac{\partial (\rho_{fume} u_{fume} c_{fume} T)}{\partial r} + k_{eff} \frac{\partial^2 T}{\partial z^2} + \frac{1}{r} \frac{\partial (k_{eff} r \partial T / \partial r)}{\partial r} + Q = 0 \tag{3}$$

where c_s and c_{fume} are the specific heat capacity of solid and fume (J/(kg · K)), respectively; T is the temperature (K); k_{eff} is the effective conductivity of solid (W/(m · K)); Q is the heat source rate (kJ/(m^3 · s)) and has different expressions in various control vol-

umes.

1.2.2 Items in governing equation

Effective conductivity: Effective heat conduction includes heat conduction and radiation. As the result, effective heat conduction is expressed as Eq. (4).

$$k_{\text{eff}} = k_{\text{T}} + 4\varphi\varepsilon\sigma T^3 l_{\text{r/a}} \tag{4}$$

where k_{T} is the conductivity of solid (W/(m · K)), and its value is linear with temperature ($k = k_0 + sT$) [37]; φ is the porosity; ε is the emissivity; σ is the Stephen-Boltzmann constant (W/(m^2 · K^4)); $l_{\text{r/a}}$ is the radial and axial length of control volume (m).

Propagation velocity: The smoldering propagation velocity is calculated according to literature[18].

$$u_{\text{sm}} = \frac{\rho_{\text{a}} Y_{\text{O}_2}}{\gamma\rho_{\text{f}}} u_{\text{a}} = \frac{\rho_{\text{a}} Y_{\text{O}_2}}{\gamma\rho_{\text{f}}} Nu \frac{\alpha}{d} \tag{5}$$

where ρ_{f} and ρ_{a} are the density of biomass rod and air (kg/m^3), respectively; Y_{O_2} is the oxygen mass fraction; γ is the stoichiometric coefficient of oxygen; u_{a} is the velocity of internal airflow inside the conical porous char (m/s); α is the thermal diffusivity (m^2/s); d is the diameter (m).

Nusselt number[38] is calculated using Eq. (6).

$$Nu = 0.59\left(Gr \cdot Pr\right)^{1/4} \quad \left(1.43\times10^4 \leqslant Gr \leqslant 3.00\times10^9\right) \tag{6}$$

where Gr is calculated using Eq. (7).

$$Gr = \frac{g\alpha_{\text{v}}\Delta T l_{\text{c}}^3}{\nu^2} \tag{7}$$

where g is the gravitational acceleration (m/s^2); α_{v} is the expansion coefficient (K^{-1}); ΔT is the temperature difference between solid and air (K); l_{c} is the characteristic length (m); ν is the kinematic viscosity (m^2/s).

Thus the propagation velocity can be determined as Eq. (8).

$$u_{\text{sm}} = \frac{\rho_{\text{a}} Y_{\text{O}_2}}{\gamma\rho_{\text{f}}} \times 0.59 \left(\frac{g\alpha_{\text{v}}\Delta T l_{\text{c}}^3}{\nu^2} \cdot Pr \right)^{1/4} \frac{\alpha}{d} \tag{8}$$

1.2.3 Source terms and fume flow inside control volume

Control volume of char oxidation: Char oxidation occurs on an internal surface[39] in the control volume of char oxidation as Eq. (9). It should be noted that at a certain z, there is only one control volume of char oxidation.

$$\text{C} + \gamma\text{O}_2 \rightarrow 2(1-\gamma)\text{CO} + (2\gamma-1)\text{CO}_2 \tag{9}$$

The molar reaction rate of carbon equals the molar production rate of fume, as shown in Eq. (10). It depends on the diffusion molar flux of oxygen ($\dot{n}_{\text{O}_2}$), as shown in Eq. (11).

$$\dot{\omega}_{\text{s}} = \frac{\dot{\omega}_{\text{fume}} M_{\text{C}}}{\gamma M_{\text{O}_2}} = \frac{\dot{n}_{\text{O}_2} \cdot M_{\text{C}}}{\gamma} \tag{10}$$

$$\dot{n}_{\text{O}_2} = \frac{c_{\text{O}_2}}{M_{\text{O}_2}\left(R_{\text{tra}} + R_{\text{kin}}\right)\text{d}r} \tag{11}$$

where M_{C} and M_{O_2} are the molar mass of carbon and oxygen (kg/mol), respectively; c_{O_2} is the oxy-gen concentration (kg/m^3); R_{tra} and R_{kin} are the trans-port and kinetics resistance (s/m), respectively.

In the control volume of char oxidation, the heat source rate Q is

$$Q = \dot{\omega}_{\text{s}} \Delta H_{\text{c}} \tag{12}$$

where ΔH_{c} is the reaction heat of char oxidation (kJ/kg).

Control volume of pyrolysis: For simplification, pyrolysis in the control volume of pyrolysis is expressed as Eq. (13) [39], and volatiles mainly include CO, CO_2, CH_4, and H_2.

$$\text{Biomass} + \Delta H_{\text{p}} \rightarrow 0.64\text{volatiles} + 0.36\text{char} \tag{13}$$

where ΔH_{p} is the reaction heat of pyrolysis (kJ/kg).

The mass reaction rate of original fuel (Eq. (1)) is equal to the mass production rate of volatiles (Eq. (2)), as shown in Eq. (14). It depends on the pyrolysis reaction rate, as shown in Eq. (15).

$$\dot{\omega}_{\rho,\text{fume}} = \dot{\omega}_{\rho,\text{s}} \tag{14}$$

$$\dot{\omega}_{\rho,\text{s}} = X_{\text{p}} \rho_{\text{f}} A_{\text{p}} \exp\left(-\frac{E_{\text{p}}}{RT_{\text{p}}} \right) \tag{15}$$

where X_{p} is the mass fraction of volatile matter in control volume; ρ_{f} is the density of fuel (kg/m^3); A_{p}, E_{p} and T_{p} are the pre-exponential factor (s^{-1}), activation energy (J/mol), and temperature (K) of pyrolysis, respectively; R is the universal gas constant (J/(mol · K)).

In the control volume of pyrolysis, the heat source rate Q is

$$Q = \dot{\omega}_{\rho,\text{s}} \Delta H_{\text{p}} \tag{16}$$

Control volume of ash outside char cone: The part of heat is entrained out due to the outflow of fume in this control volume. The $\rho_{\text{fume}} u_{\text{fume}}$ in Eq. (3) is

$$\rho_{\text{fume}} u_{\text{fume}} = \frac{c_{\text{O}_2} M_{\text{C}}}{\gamma M_{\text{O}_2}\left(R_{\text{tra}} + R_{\text{kin}}\right)} \tag{17}$$

In the control volume of ash outside char cone, the heat source rate Q is zero.

1.2.4 Boundary condition

On the top surface ($z=0$), the heat loss is composed of convection and radiation heat transfer (Eq. (18)). For the cylindrical surface ($r=d/2$), the boundary condition is the same as that on the top surface, as shown in Eq. (19). On the bottom surface ($z=0$), the adiabatic boundary condition is applied, as shown in Eq. (20). For the symmetrical plane ($r=0$), the boundary condition is the same as that on the bottom surface (Eq. (21)).

$$k_{\text{eff}}\left.\frac{\partial T}{\partial z}\right|_{z=0}=h\left(T-T_{\text{a}}\right)+\varepsilon\sigma\left(T^4-T_{\text{a}}^4\right) \tag{18}$$

$$k_{\text{eff}}\left.\frac{\partial T}{\partial r}\right|_{r=d/2}=h\left(T-T_{\text{a}}\right)+\varepsilon\sigma\left(T^4-T_{\text{a}}^4\right) \tag{19}$$

$$\left.\frac{\partial T}{\partial z}\right|_{z=l}=0 \tag{20}$$

$$\left.\frac{\partial T}{\partial z}\right|_{r=0}=0 \tag{21}$$

where T_{a} is the ambient temperature, K; h is the convective heat transfer coefficient between air and dried biomass rod (W/(m^2 · K)).

1.3 Parameters

The parameters and values involved in the calculation are given in Tab.1.

Tab.1 Parameters involved in the calculation

Parameter	Value
A_{c}/(m · s^{-1})	6 655 [40]
E_{c}/(J · mol^{-1})	91.5 × 10^3 [40]
A_{p}/(m · s^{-1})	2 × 10^5 [35]
E_{p}/(J · mol^{-1})	120 × 10^3 [35]
R/(J · kg^{-1} · K^{-1})	8.314
ΔH_{c}/(kJ · kg^{-1})	2.1 × 10^4 [Eq. 6]
ΔH_{p}/(kJ · kg^{-1})	− 570 [35]
ρ_{f}/(kg · m^{-3})	471.3
c_s/(J · kg^{-1} · K^{-1})	1 200
k_0	0.2[39]
s	0.002 [Estimated]
h/(W · m^{-2} · K^{-1})	8.4 [41]
ε	0.9[39]
σ/(W · m^{-2} · K^{-4})	5.67 × 10^{-8}
Y_{O_2}	0.23[42]
γ	0.7[43]

1.4 Numerical method

1.4.1 Cells

The finite volume approach is applied in this work. The simulation domain is divided into cells, including top cells, ash cells, oxidation cells, char cells, pyrolysis cells, bottom cells, central cells, and cylindrical surface cells, as shown in Fig.2(a). The radius of the whole computational domain is evenly divided into *nr* cells, and the rod length is divided into *nz* cells. The radial cells are numbered from 1 to *nr* from the center outwards and expressed by *i*. Similarly, the axial cells are numbered from 1 to *nz* from top to bottom and expressed by *j*. It should be noted that the relationship between dz and dr in oxidation cells is shown in Eq. (22). In other cells, the value of dz and dr is equal.

$$\frac{\text{d}z}{\text{d}r}=\frac{\gamma\rho_{\text{c}}u_{\text{sm}}\left(R_{\text{tra}}+R_{\text{kin}}\right)}{M_{\text{C}}c_{\text{O}_2}} \tag{22}$$

where ρ_{c} is the density of carbon, kg/m^3.

1.4.2 Solution procedure

The 2D steady model of smoldering is solved by self-written program using MATLAB software. The solution procedure of model is shown in Fig.2(b). The properties, constants and operation condition parameters are input firstly. Then the temperature and density of biomass rod are initialized. The *Gr* and *Nu* numbers are calculated by the given qualitative temperature and characteristic length, and the propagation velocity is calculated by Eq. (8). The char cone shape is calculated by Eq. (22). Then the mass and energy equations are iteratively solved by semi-implicit method. When the iterative errors of temperature filed, density filed, and char cone length meet the requirements, the inner iteration is ended. Then it is judged whether the qualitative temperature iteration error meets the requirements. If not, temperature and density initialization is returned, otherwise the outer iteration ends and the data is recorded.

1.4.3 Independence analysis of model grid

The value of *nr* affects the number of model grid. The different smoldering characteristics of biomass rod with the diameter of 4.8 mm changing with different *nr* is shown in Fig.3. It can be seen that the results have little difference (maximum error < 1%) when *nr* is 30, 40 and 50. Thus *nr* is taken as 30 to reduce the calculation cost.

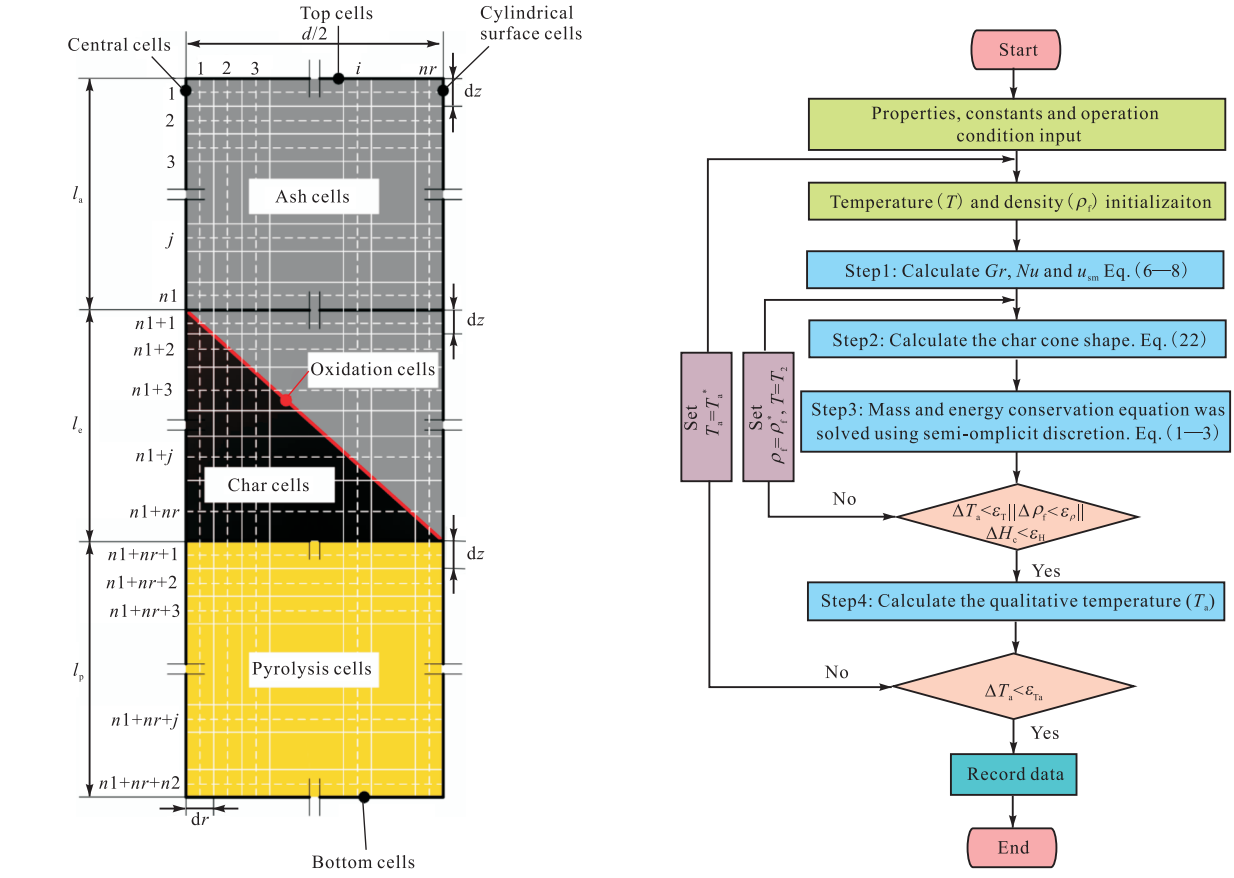

(a) Cells (b) Solution procedure

Fig.2 Cells and solution procedure

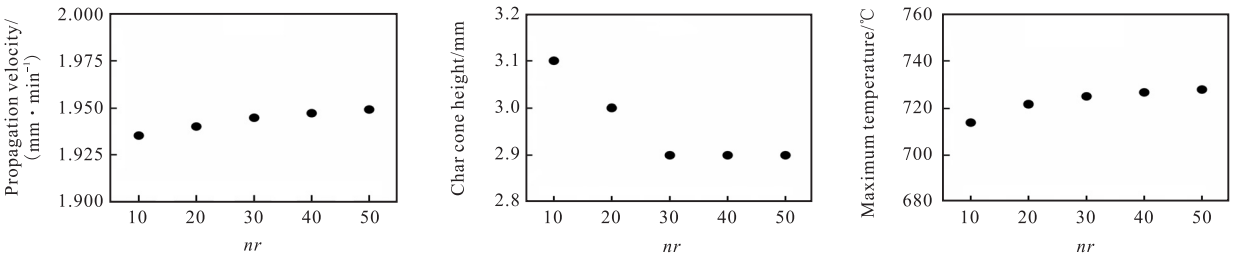

(a) Propagation velocity (b) Char cone height (c) Maximum temperature

Fig.3 Independence analysis of model grid based on propagation velocity, char cone height and maximum temperature

2 Experiments

2.1 Samples preparation

Biomass rods extruded from the wet mixture of pine powder and elm bark powder were prepared at the planned diameter of 3 mm, 5 mm, 8 mm. The detailed preparing process is seen in literature[44]. The diameter of the experimental rods is 2.9 mm, 4.8 mm and 7.6 mm, respectively. The ash, volatile, fixed carbon content, and density of biomass rods are 10.55% , 67.23% , 22.22% , and 471.3 kg/m^3, respectively.

2.2 Procedure of the experiments

The propagation velocity, char cone shape, and temperature field are measured in Fig.4[44]. It should be noted that the emissivity of biomass rod is 0.9 in infrared image analysis.

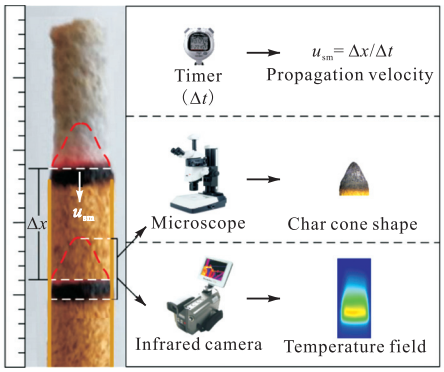

Fig.4 Schematic diagram of the experiments[44]

3 Results and discussion

3.1 Calculated results

The comparisons of smoldering characteristics between calculation and experiments are shown in Fig.5.

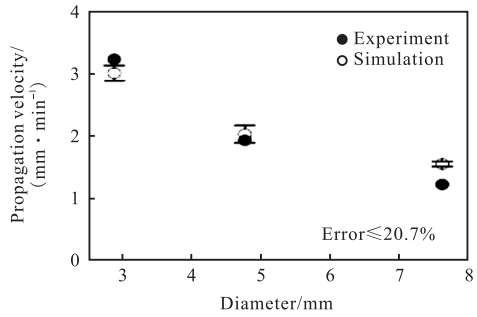

(a) Propagation velocity

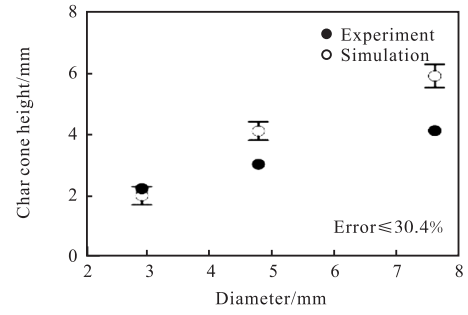

(b) Char cone height

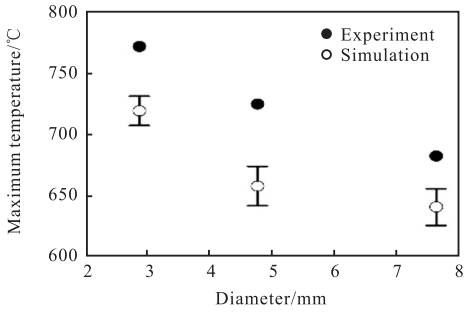

(c) Maximum temperature

Fig.5 Comparison of numerically calculated and experimentally measured propagation velocity char cone height and maximum temperature

3.1.1 Propagation velocity

As displayed in Fig.5(a), the error between the calculated and experimental results is the smallest when the diameter is 4.8 mm, and the maximum error is about 20.7% when the diameter is 7.6 mm. The propagation velocity of both is in the same order of magnitude as that of incense (3.2—6.5 mm/min) in literature[18-30], and both are lower than 4 mm/min. It should be noted that the selected characteristic length in Eq. (7) is the sum of the lengths of ash rod and char cone. The value of characteristic length could affect propagation velocity, which will be further studied in the future work.

3.1.2 Char cone height

From Fig.5(b), it is seen that the error between the calculated and experimental results increases with increasing diameter, and the maximum error is about 30.4% as the diameter is 7.6 mm. During the experimental measurement, it is difficult to clearly distinguish the boundary between the char cone and pyrolysis zone, resulting in a larger error in the experimental value of char cone height.

3.1.3 Maximum temperature

The calculated and experimental values of maximum temperature are shown in Fig.5(c). It should be noted that the calculated and experimental temperature is the internal temperature and surface temperature of biomass rod, respectively. Therefore, the values of both calculation and experiment are only used for comparison and not for the verification of the reasonability of model. The maximum temperature range of experiment is between 630—730 ℃, which is close to the value in literature[30-35], and the maximum calculated temperature is about 50 ℃ higher than the experimental value.

From the above discussions, considering the complex nature of steady smoldering, the calculation predictions and experimental data agree reasonably well.

3.2 Sensitivity analysis

3.2.1 Effect of diameter

It is found from our pre-experiment that the diameter of dried biomass rod might affect the smoldering characteristics. Thus, dried biomass rods with different diameters of 2 mm, 2.9 mm, 4.8 mm, 7.6 mm, and 10 mm are chosen to study the effect of diameter.

The effects of diameter on the smoldering characteristics are shown in Fig.6. It is seen that the propagation velocity decreases from 4.73 mm/min to 0.96 mm/min as the diameter increases from 2 mm to 10 mm, as shown in Fig.6(a). and the trend is consistent with the literature[18]. Such a trend can also be explained by Eq. (8), where the propagation velocity is inversely proportional to diameter. As shown in Fig.6(b), the char cone height H_c increases from 1.7 mm to 5.1 mm.

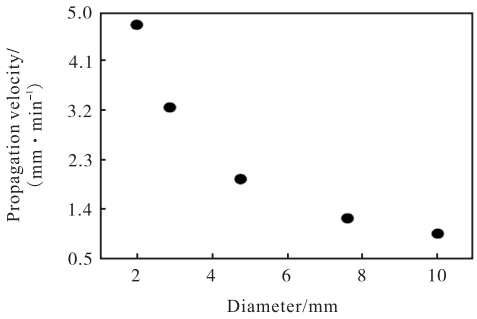

（a）Propagation velocity

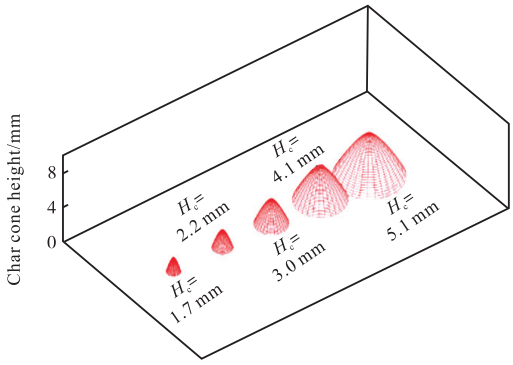

（b）Char cone

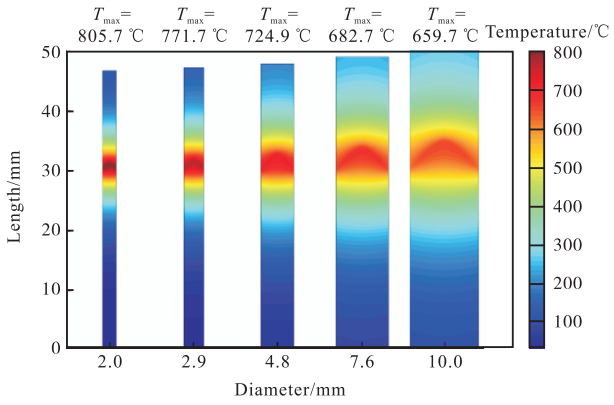

（c）Temperature field

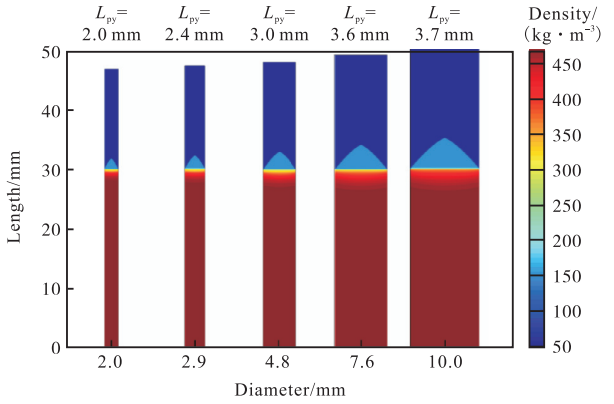

（d）Density field

Fig.6 Effects of rod diameter on smoldering propagation velocity char cone temperature field and density field

On the contrary, the maximum temperature T_{max} decreases from 805.7 ℃ to 659.7 ℃ with increasing diameter, but the range of high temperature region increases. At the same time, the pyrolysis zone length L_{py} (the distance from the bottom of char cone to the area where the mass of original fuel decreases by 1%) increases by 0.85 times from 2.0 mm to 3.7 mm, obviously.

3.2.2 Effect of density

The density of biomass rods may change during laboratory production, and thus affect the smoldering characteristics. Taking the dried biomass rod with a diameter of 4.8 mm as an example, the smoldering process at different density of 450 kg/m^3, 471.3 kg/m^3, 500 kg/m^3, 525 kg/m^3, and 550 kg/m^3 is studied.

The effects of density on the smoldering characteristics are summarized in Fig.7. As the density increases from 450 kg/m^3 to 550 kg/m^3, the propagation velocity decreases from 2.04 mm/min to 1.66 mm/min. As ex-pected, the result agrees with the theoretical analysis of Eq. (8) where the propagation velocity is inversely proportional to the density. Such a trend of propagation velocity is consistent with that in literature[18]. The char cone height increases slightly at the early stage with increasing density, but it is unaffected when the density reaches 471.3 kg/m^3. The effect of density on the maximum temperature and pyrolysis zone length is ignoreable. The results may be related to the heat balance during smoldering.

3.2.3 Effect of oxygen mass fraction

The oxygen supply dominates the smoldering process of rod fuel[18, 35]. Taking the dried biomass rod with a diameter of 4.8 mm as an example, the smoldering process at different oxygen mass fraction of 0.17, 0.19, 0.21 0.23, and 0.25 is studied.

The effects of oxygen mass fraction on the smoldering characteristics are presented in Fig.8. As shown in Figs.8 (a) and (b), both propagation velocity and char cone height are significantly affected by oxygen mass fraction. As the oxygen mass fraction increases from 0.17 to 0.25, the propagation velocity increases by 0.62 times from 1.34 mm/min to 2.17 mm/min. At the same time, the char cone height increases by 0.32 times from 2.5 mm to 3.3 mm. It is consistent with the smoldering process in literature, a faster smoldering propagation and longer luminous region for

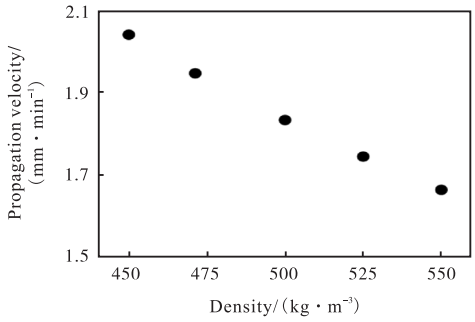

(a) Propagation velocity

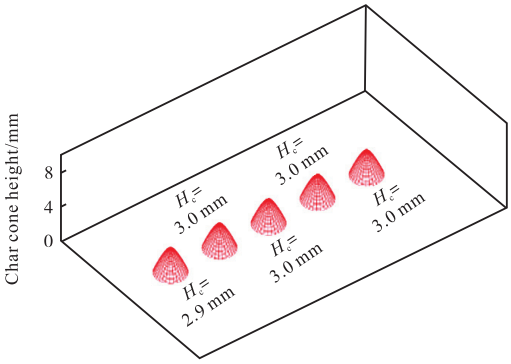

(b) Char cone

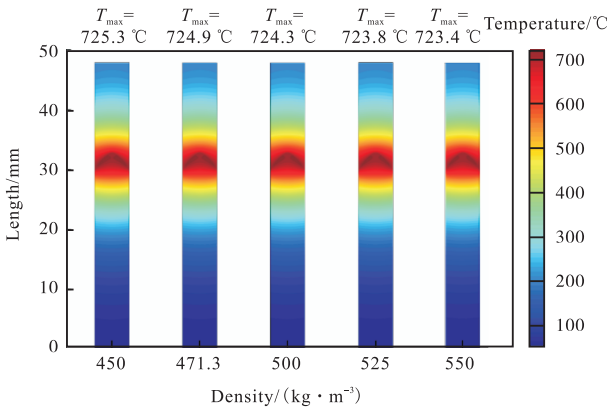

(c) Temperature field

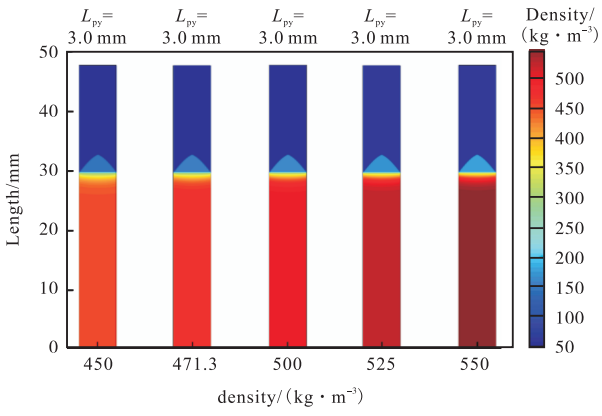

(d) Density field

Fig.7 Effects of density on smoldering propagation velocity char cone temperature field and density field

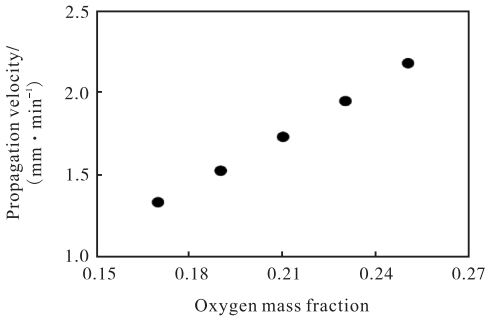

(a) Propagation velocity

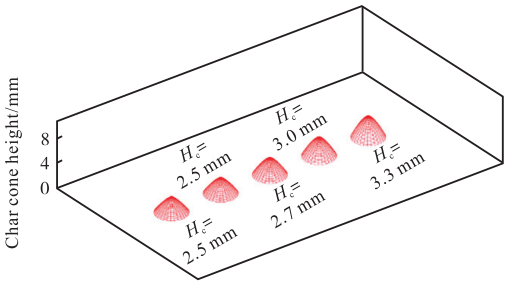

(b) Char cone

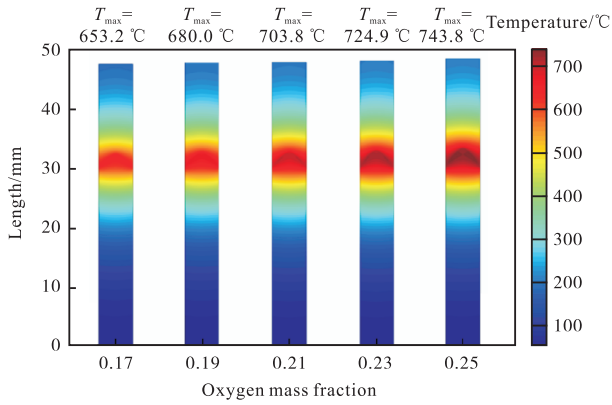

(c) Temperature field

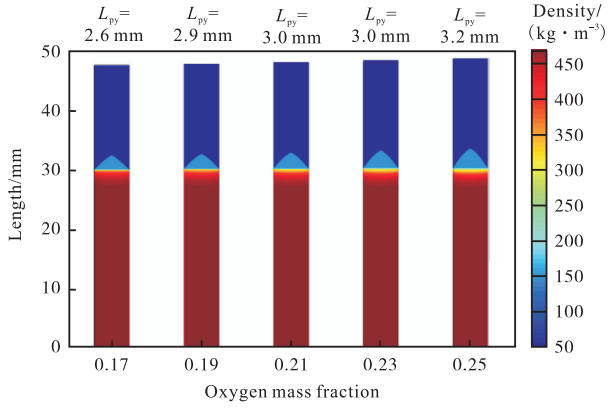

(d) Density field

Fig.8 Effects of oxygen mass fraction on smoldering propagation velocity char cone temperature field and density field

a lager oxy-gen mass fraction[30-31,35]. The maximum temperature also increases from 653.2 ℃ to 743.8 ℃ with increasing oxygen mass fraction. The trend is in agreement with that in literature[35]. The pyrolysis zone length increases from 2.6 mm to 3.2 mm as the oxygen mass fraction increases from 0.17 to 0.25.

3.2.4 Comparison of the sensitivity of factors

The sensitivities of factors are compared using a mean sensitivity coefficient[45] (SN), as shown in Eq. (23).

$$SN=\frac{1}{n-1}\sum_{i=1}^{n}\frac{(y_{i+1}-y_i)/y_i}{(x_{i+1}-x_i)/x_i} \tag{23}$$

where x is the value of factor; y is the value of typical characteristics of process; n is the number of factor. Taking the absolute value of SN, the sensitivity coefficient can be divided into three grades[45]: $|SN|>0.2$ is a strong sensitivity coefficient, $0.1<|SN|<0.2$ is a medium sensitivity coefficient, and $|SN|<0.1$ is a low sensitivity coefficient. The parameter corresponding to the three sensitivity coefficients is one with strong, medium, and low effect.

The sensitivity of smoldering characteristics to different parameters is shown in Fig.9. Diameter, density, and oxygen mass fraction have a strong effect on propagation velocity. However, only oxygen mass fraction has a promoting effect. Both diameter and oxygen mass fraction have a strong effect on char cone height, while density has a medium effect on it. Oxygen mass fraction has a strong promoting effect on maximum temperature, while the effect of diameter and density is ignorable. The pyrolysis zone length is very sensitive to diameter and oxygen mass fraction, but not sensitive to density. It can be predicted that increasing the diameter of rod fuel can decrease the propagation velocity and increase the length of oxidation area and pyrolysis zone significantly.

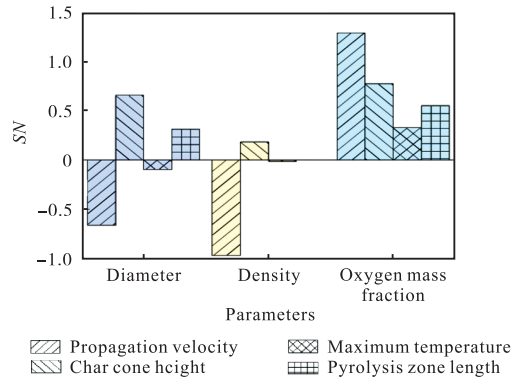

Fig.9 Sensitivity of smoldering characteristics to different parameters

4 Conclusion

On the basis of our previous experiments on and empirical correlation with propagation velocity from literature, a 2D steady model of smoldering biomass rods was developed and numerically analyzed. Results show that the calculation results agree well with the experimental observation, and the maximum error is smaller than 31%.

Sensitivity analysis shows that only oxygen mass fraction significantly promotes propagation velocity. Diameter, density, and oxygen mass fraction have promoting effect on char cone height. Oxygen mass fraction has a strong promoting effect on maximum temperature, while the effect of diameter and density is ignorable. The pyrolysis zone length is very sensitive to diameter and oxygen mass fraction, but not sensitive to density. Prediction shows that propagation velocity decreases significantly while oxidation area and pyrolysis zone increase significantly with increasing diameter of rod fuel.

The model provides a tool for deeper understanding of steady smoldering process, and future work on more accurate propagation velocity is necessary.

Acknowledgements

The authors acknowledge the financial supports provided by Sino-German Center for Research Promotion (Grant No. M-0183), Natural Science Foundation of Shandong (Grant No. ZR2022ME038), and Innovation ability improvement project of small and medium-sized technology-based enterprises (Grant No. 2021TSGC1114).

Nomenclature

Symbols

A— pre-exponential factor of pyrolysis, s^{-1};

c— specific heat capacity, J/(kg · K);

d— diameter of dried biomass rod, m;

E— activation energy of pyrolysis, J/mol;

Gr— Grashof number;

h— convective coefficient, W/(m^2 · K);

ΔH— reaction heat, kJ/kg;

k— thermal conductivity, W/(m · K)

Nu— Nusselt number;

Pr— Prandtl number;

Q— heat source term, kJ/(m^3 · s);

R— universal gas constant, J/(mol · K);

r— radius, m;

T— temperature, K;

u— velocity, m/s;

Y— mass fraction.

Greeks

α— thermal diffusivity, m^2/s;

α_v— expansion coefficient, (K^{-1});

γ— oxygen stoichiometric coefficient;

ε— emissivity;

v— kinematic viscosity, m^2/s;

ρ— density, kg/m^3;

σ— Stephen-Boltzmann constant, W/(m^2 · K^4);

φ— porosity;

$\acute{\omega}$— mass source term, kg/(m^3 · s).

Subscripts

a— air/ash;

c— carbon/char;

eff—effective heat conductivity;

f— fuel;

g— gas;

i— reaction number;

kinv— kinetics;

O_2— oxygen;

p— pyrolysis;

s— solid;

sm— smoldering;

tra— mass transfer;

v— volatile.

Reference

[1] Torero J L, Gerhard J I, Martins M F, et al. Processes defining smouldering combustion: Integrated review and synthesis[J]. *Progress in Energy and Combustion Science*, 2020, 81: 100869.

[2] Ohlemiller T J. Modeling of smoldering combustion propagation[J]. *Progress in Energy and Combustion Science*, 1985, 11(4): 277-310.

[3] Pan Junjie, Li Jun. Basic characteristics of smoldering process in coal packed bed under natural ventilation[J]. *Journal of Combustion Science and Technology*, 2022, 28(5): 583-590.

[4] Ohlemiller T J. Smoldering combustion[J]. *SFPE Handbook of Fire Protection Engineering*, 2002, 3: 200-210.

[5] Gianfelice G, Della Zassa M, Biasin A, et al. Onset and propagation of smouldering in pine bark controlled by addition of inert solids[J]. *Renewable Energy*, 2019, 132: 596-614.

[6] Rashwan T L, Fournie T, Torero J L, et al. Scaling up self-sustained smouldering of sewage sludge for waste-to-energy[J]. *Waste Management*, 2021, 135: 298-308.

[7] Liang Zhirong, Chen Yuying, Lin Shaorun, et al. Emission characteristics of smoldering combustion of peat[J]. *Journal of Combustion Science and Technology*, 2023, 29(4): 429-434.

[8] He F, Yi W, Zha J. Measurement of the heat of smoldering combustion in straws and stalks by means of simultaneous thermal analysis[J]. *Biomass and Bioenergy*, 2009, 33(1): 130-136.

[9] He F, Yi W, Li Y, et al. Effects of fuel properties on the natural downward smoldering of piled biomass powder: Experimental investigation[J]. *Biomass and Bioenergy*, 2014, 67: 288-296.

[10] Zhao C, Li Y, Gan Z, et al. Method of smoldering combustion for refinery oil sludge treatment[J]. *Journal of Hazardous Materials*, 2021, 409: 124995.

[11] Song Z, He T, Li M, et al. Self-sustaining smoldering as a novel disposal approach for food waste with high moisture content[J]. *Fuel Processing Technology*, 2022, 228: 107144.

[12] Ohlemiller T J. Modeling of smoldering combustion propagation[J]. *Progress in Energy and Combustion Science*, 1985, 11(4): 277-310.

[13] Yang J, Liu N, Chen H, et al. Effects of atmospheric oxygen on horizontal peat smoldering fires :

Experimental and numerical study[J]. *Proceedings of the Combustion Institute*, 2019, 37(3): 4063-4071.

[14] Zanoni M A B, Torero J L, Gerhard J I. Experimental and numerical investigation of weak, self-sustained conditions in engineered smouldering combustion[J]. *Combustion and Flame*, 2020, 222: 27-35.

[15] Dodd A B, Lautenberger C, Fernandez-Pello C. Computational modeling of smolder combustion and spontaneous transition to flaming[J]. *Combustion and Flame*, 2012, 159(1): 448-461.

[16] Fernandez-Anez N, Meyer A K, Elio J, et al. Behaviour of smoldering fires during periodic refilling of wood pellets into silos[J]. *Journal of Loss Prevention in the Process Industries*, 2021, 72: 104565.

[17] Lu Z. A diffusion-flame analog of forward smolder waves: (I) 1-D steady structures[J]. *Combustion and Flame*, 2018, 196: 515-528.

[18] Lin S, Chow T H, Huang X. Smoldering propagation and blow-off on consolidated fuel under external airflow[J]. *Combustion and Flame*, 2021, 234: 111685.

[19] Rein G, Huang X. Smouldering wildfires in peatlands, forests and the arctic: Challenges and perspectives[J]. *Current Opinion in Environmental Science & Health*, 2021, 24: 100296.

[20] Huang X, Lin S, Liu N. A review of smoldering wildfire: Reasearch advances and prospects[J]. *Journal of Engineering Thermophysics*, 2021, 42(2): 512-528.

[21] Fournie T, Rashwan T L, Switzer C, et al. Smouldering to treat PFAS in sewage sludge[J]. *Waste Management*, 2023, 164: 219-227.

[22] Zha W, Lin B, Liu T. Effect of high temperature heat source characteristics on smoldering propagation characteristics of wood powder[J]. *Journal of Engineering Thermophysics*, 2019, 40(11): 2664-2671.

[23] Yu K, Bai L, Zhang T, et al. Improving the thermal performance of the traditional Chinese Kang system by employing smoldering combustion and mechanical ventilation: An experimental study[J]. *Energy and Buildings*, 2022, 256: 111736.

[24] Yang T, Lin S, Lin T, et al. Characterization of polycyclic aromatic hydrocarbon emissions in the particulate and gas phase from smoldering mosquito coils containing various atomic hydrogen/carbon ratios[J]. *Science of the Total Environment*, 2015, 506-507: 391-400.

[25] Huang X, Gao J. A review of near-limit opposed fire spread[J]. *Fire Safety Journal*, 2021, 120: 103141.

[26] Vivekanandhan P, Senthil-Nathan S, Shivakumar M S. Larvicidal, pupicidal and adult smoke toxic effects of Acanthospermum hispidum (DC) leaf crude extracts against mosquito vectors[J]. *Physiological and Molecular Plant Pathology*, 2018, 101: 156-162.

[27] Tayel A A. Innovative system using smoke from smoldered plant materials to control Aspergillus flavus on stored grain[J]. *International Biodeterioration & Biodegradation*, 2010, 64(2): 114-118.

[28] Wu H C, Chen Y C, Hsieh C L, et al. Chemical constituents and their anti-neuroinflammatory activities from the bark of Taiwan incense cedar, Calocedrus formosana[J]. *Phytochemistry*, 2022, 204: 113347.

[29] Hasheminia S, Sho'ouri N. The effect of musk incense stick aroma inhalation on different features of electroencephalogram signals and working memory for use in neurofeedback training[J]. *Biomedical Signal Processing and Control*, 2023, 83: 104658.

[30] Yamazaki T, Matsuoka T, Li Y, et al. Applicability of a low-pressure environment to investigate smoldering behavior under microgravity[J]. *Fire Technology*, 2019, 56(1): 209-228.

[31] Yan Shengtai, Zhao Wentao, Zhang Yi, et al. Effect of combustion propagation velocity on shape of reaction cone in a char rod[J]. *Journal of Combustion Science and Technology*, 2023, 29(6): 693-698.

[32] Mukunda H S, Basani J, Shravan H M, et al. Smoldering combustion of "incense" sticks—Experiments and modeling[J]. *Combustion Science and Technology*, 2007, 179(6): 1113-1129.

[33] Yan S, He F, Cai J, et al. Characteristics of char cone covered by ash in steady smoldering of a char rod[J].

Combustion Science and Technology，2022：10.1080/00102202. 2022. 2150079 .

［34］Yamazaki T，Matsuoka T，Kuwana K，et al. Study on the flaming-transition behavior of a downwardly smoldering biomass stick utilizing low pressure［J］. *Proceedings of the Combustion Institute*，2021，38（3）：5073-5080.

［35］Kadowaki O，Suzuki M，Kuwana K，et al. Limit conditions of smoldering spread in counterflow configuration：Extinction and smoldering-to-flaming transition［J］. *Proceedings of the Combustion Institute*，2021，38（3）：5005-5013.

［36］Rostami A，Murthy J，Hajaligol M. Modeling of a smoldering cigarette［J］. *Journal of Analytical and Applied Pyrolysis*，2003，66（1）：281-301.

［37］Yin L，Xiao Y，LI Q，et al. Temperature effect on thermal conductivity of oxidised coal associated with its predictive model during coal pyrolysis［J］. *Energy*，2023，274：127417.

［38］Yang S，Zhang Z. An experimental study of natural convection heat transfer from a horizontal cylinder in high rayleigh number laminar and turbulent regions［C］// 10th *International Heat Transfer Conference*. Brighton，Britain，1994：185-189.

［39］He F，Behrendt F. A new method for simulating the combustion of a large biomass particle—A combination of a volume reaction model and front reaction approximation［J］. *Combustion and Flame*，2011，158（12）：2500-2511.

［40］Li X，He F，Cai J，et al. Oxidation kinetics of maize stover char at low temperature based on surface area and temperature correction［J］. *Energy*，2022，241：122928.

［41］Di Blasi C. Analysis of convection and secondary reaction effects within porous solid fuels undergoing pyrolysis［J］. *Combustion Science and Technology*，1993，90（5-6）：315-340.

［42］He F，Zobel N，Zha W，et al. Effects of physical properties on one-dimensional downward smoldering of char：Numerical analysis［J］. *Biomass and Bioenergy*，2009，33（8）：1019-1029.

［43］Ronda A，Della Zassa M，Gianfelice G，et al. Smouldering of different dry sewage sludges and residual reactivity of their intermediates［J］. *Fuel*，2019，247：148-159.

［44］Zhao W，Zhang Y，Yu G，et al. Comparison on the steady smoldering characteristics of char and biomass rods［J］. *Transactions of the Chinese Society of Agricultural Engineering*，2023，39（8）：1-7.

［45］Tatarinov F A，Cienciala E. Application of BIOME-BGC model to managed forests［J］. *Forest Ecology and Management*，2006，237（1）：267-279.